American Mineralogist, Volume 100, pages 2043–2052, 2015

SPECIAL COLLECTION: OLIVINE

Phosphoran olivine overgrowths: Implications for multiple impacts to the Main Group pallasite parent body†

Neva A. Fowler-Gerace[1,*] and Kimberly T. Tait[1,2]

[1]Department of Earth Sciences, University of Toronto, 22 Russell Street, Toronto, Ontario M5S 3B1, Canada
[2]Department of Natural History, Mineralogy, Royal Ontario Museum, 100 Queens Park, Toronto, Ontario M5S 2C6, Canada

Abstract

Phosphoran olivine (1–7 wt% P_2O_5) is a metastable phase known from fewer than a dozen meteoritic or terrestrial occurrences. We have thoroughly examined phosphoran olivine in the Springwater pallasite to characterize its distribution, textural relationships, and geochemistry. Phosphoran olivine is abundant in Springwater as randomly distributed millimeter-scale partial overgrowths on the P-free olivine crystals. Geochemical analyses support the substitution mechanism of P into the tetrahedral Si site with octahedral site vacancies for charge balance; observed trace element variations, on the other hand, are not related to P substitution. Element mapping reveals fine-scale oscillatory P zoning in unusual serrate patterns, indicating rapid crystal nucleation from a melt as proposed by Boesenberg and Hewins (2010) and a subsequently variable rate of crystallization. The timing of phosphoran olivine formation in Springwater is constrained to after the period of macroscopic olivine rounding but before the cooling of the metal matrix; because the phosphoran overgrowths overprint specific host grain boundary modifications, we suggest that the episode of extremely rapid cooling necessary to crystallize and preserve this rare phase may have been triggered by an additional impact to the parent body.

Keywords: Phosphoran olivine, Springwater pallasite, petrography

Introduction

Terrestrial igneous olivine typically contains <0.01–0.04 wt% P_2O_5 (Milman-Barris et al. 2008); occasionally, however, the phase can host orders of magnitude more phosphorus. Olivine containing 1–7 wt% P_2O_5—generally termed "phosphoran olivine" (e.g., Boesenberg and Hewins 2010)—is known from nearly a dozen separate occurrences (Buseck 1977; Buseck and Clark 1984; Goodrich 1984, 2003; Agrell et al. 1998; Wasson et al. 1999; Tropper et al. 2004; Boesenberg 2006; Wang et al. 2007), all but four of which (Goodrich 1984; Agrell et al. 1998; Tropper et al. 2004; Boesenberg 2006) are extraterrestrial. Up to 32 wt% P_2O_5 has been reported in olivine from secondary melt inclusions in the Brahin pallasite meteorite (Sonzogni et al. 2009).

Because the olivine/melt partition coefficient for P is only 0.001–0.1 (Anderson and Greenland 1969; Brunet and Chazot 2001; Boesenberg and Hewins 2010), the presence of several wt% P_2O_5 in olivine suggests extenuating circumstances. Boesenberg and Hewins (2010) have experimentally determined that under rapid crystallization regimes P behaves as if it is compatible in olivine, producing a metastable phosphoran olivine phase that will persist only if cooling below the solidus occurs within several weeks. Olivine may accommodate significant amounts of P through substitution of P^{5+} for Si^{4+} in the tetrahedral site while Mg^{2+} and Fe^{2+} vacancies in the octahedral site balance charge (Buseck and Clark 1984; Boesenberg and Hewins 2010). Substitutions involving Li^+ and Na^+ (Mallmann et al. 2009) or trivalent cations (Milman-Barris et al. 2008) have been shown to facilitate P incorporation into olivine at trace levels; however, the latter mechanism may not operate in even low-P pallasite olivine given a lack of definitive correlations between P and Cr, Al, Ti, V, Sc, or Ga in the Brenham and Brahin pallasites (McKibbin et al. 2013).

It is not known whether rapid crystallization is the only atypical condition required to form phosphoran olivine. The experimental data suggest it can crystallize under the same temperature, composition, and oxygen fugacity parameters as nominally P-free olivine (Boesenberg and Hewins 2010). Still, phosphoran olivine is extremely rare in nature, with five of its reported occurrences in the considerably unusual phase assemblage of pallasite meteorites: primarily large forsteritic olivine grains suspended within an iron-nickel matrix, with accessory phosphates, troilite (FeS), schreibersite [$(Fe,Ni)_3P$], and chromite. Some workers have suggested pallasitic phosphoran olivine formed below its solidus, following oxidation of P from the schreibersite and metal phases during cooling (Olsen and Fredriksson 1966) and potentially involving replacement of olivine rims by reaction with adjacent phosphates (Buseck 1977). However, it has been noted more recently that a subsolidus origin of pallasitic phosphoran olivine is unlikely given the lack of diffusion profiles within the adjacent metal or P-free olivine; crystallization from a quickly cooling melt as has been achieved experimentally is therefore the most viable mechanism (Boesenberg and Hewins 2010). This cooling rate prerequisite for phosphoran olivine formation is challenging

* E-mail: neva.fowler.gerace@mail.utoronto.ca
† Special collection papers can be found on GSW at http://ammin.geoscienceworld.org/site/misc/specialissuelist.xhtml.

0003-004X/15/0010–2043$05.00/DOI: http://dx.doi.org/10.2138/am-2015-5344

to reconcile with the general assumption that pallasites formed substantially below the surface of their parent body (e.g., Buseck 1977; Scott 1977; Tarduno et al. 2012; Boesenberg et al. 2012) and contain evidence within their metal matrices for cooling rates as low as several degrees per million years (Yang et al. 2010).

Here we perform a thorough characterization of phosphoran olivine within the Springwater pallasite, a 52.8 kg sample initially recovered in 1931 near Saskatoon, Saskatchewan, Canada. Like three of the other four pallasites known to bear phosphoran olivine, Springwater contains macroscopically rounded olivine grains, a texture thought to arise through the thermodynamically favored reduction in olivine surface area during prolonged contact with the metal matrix at elevated temperatures (Scott 1977; Ohtani 1983; Saiki et al. 2003). This and other textural modifications to Springwater olivine place additional constraints on the prevailing conditions during phosphoran olivine formation and its timing relative to other events in the meteorite's history. To refine our understanding of the crystallization mechanisms, we have analyzed major, minor, and trace elements with particular focus on zoning patterns. We complement the geochemical data with detailed observations of the large-scale distribution and textural features of phosphoran olivine in Springwater to elucidate the origin of this unusual phase within the Main Group pallasite parent body.

Method

Three approximately 3 × 5 cm polished thick sections from the Springwater pallasite were examined thoroughly for phosphoran olivine. The P content of this phase is sufficiently high that it can be located using a backscattered electron image with exaggerated contrast. Two of the samples were searched systematically for phosphoran olivine using the JEOL JXA-8230 electron microprobe (EMP) at Queen's University, Kingston, Ontario, using an accelerating voltage of 15 kV, a 30 nA beam current, and a focused ≤1 μm beam. Individual occurrences were imaged and analyzed for P, Si, Ti, Al, Cr, V, Ca, Fe, Co, Mg, Mn, Ni, K, and Na. Matrix corrections were PAP [Pouchou and Pichoir 1985—double parabolic φ(ρz) function] and the mass absorptions coefficients database was MAC30 (Heinrich 1986). Additional points were analyzed for P, Si, Fe, Mg, and Mn at the University of Toronto, Ontario, with a Cameca SX-50 electron microprobe at 20 kV and 30 nA with a ~1 μm beam. Data were processed using the Armstrong (1988) matrix correction method and the CITZMU (Heinrich 1966; Henke and Ebisu 1974) mass absorption coefficients database. In both EMP data sets, analyses with oxide totals not within 99.00–101.00% were rejected.

Prior to trace element analysis, linear regions of roughly uniform P content (see description of zoning patterns in next section) were identified via element mapping using the scanning electron microscope at the University of Toronto, at an accelerating voltage of 15 kV and with a specimen current of ~6 nA. Trace elements were measured using laser ablation-inductively coupled plasma-mass spectrometry (LA-ICP-MS) at the University of Toronto. A frequency quintupled Nd:YAG laser coupled to a VG PQExcell quadrupole ICP-MS was operated at a repetition rate of 10 Hz with a 18 μm spot size (intentionally small to avoid the ablation of multiple regions differing in P content). For each analysis, 20 s of background collection while flushing the ablation cell with He were followed by 60 s of data acquisition while ablating a line in the sample. The NIST610 silicate glass standard was measured twice with a 55 μm spot before and after each set of 16 analyses, with Mn (measured using EMP as described above) used as an internal reference element to correct for ablation yields in the standard. Data were reduced using the GLITTER software package (version 4.4.4). A preliminary run included a large suite of elements (Li, Na, Al, K, Ca, Sc, Ti, V, Cr, Co, Ni, Cu, Zn, Ga, Ge, As, Se, Rb, Sr, Y, Zr, Nb, Mo, Ag, Cd, Sn, Te, Sb, Cs, La, Ce, Nd, Sm, Eu, Gd, Dy, Lu, Hf, Ta, W, Re, Au, Pb, and Bi) but most were not detectable in the phosphoran olivine. In subsequent runs many elements were eliminated from the analytical regime to increase the time spent counting on each mass. Note that Na, K, Ca, and Ni may be present at parts per million levels, given their concentrations in Springwater P-free olivine reported by Hsu (2003) and Floss (2002), but these elements are associated with high backgrounds in the NIST610 standard and therefore could not be detected in this study. Analyses with >50 ppm Co were rejected because these elevated values likely reflect contamination from the fine network of metal veining across the olivine grains [Springwater metal contains 5880 ppm Co (Wasson and Choi 2003), whereas the olivine is reported at only 2–7 ppm (Leitch et al. 1979)].

Distribution and textures

In the Springwater pallasite, phosphoran olivine occurs exclusively as epitaxial overgrowths on the nominally P-free olivine crystals (Fig. 1). A single region of phosphoran olivine identified within the central portion of an olivine grain likely represents a grain edge sectioned by the sample surface, based on concentric zoning similar to all other occurrences (described below). Phosphoran overgrowths range from 28–459 μm in width and 130–4116 μm in length, or 137 × 1421 μm on average. Phosphoran olivine is ubiquitous in Springwater, with 47% of the P-free olivine grains in the samples searched systematically bearing at least one overgrowth and 69 overgrowths observed in total. Phosphoran overgrowths occur on all three host olivine grain boundary morphologies in Springwater: rounded (the majority of grains), subplanar and complementary in shape to neighboring grains [described by Scott (1977) in the Brenham pallasite], and jagged (occasionally present on small grains) (Fig. 2). Phosphoran olivine is not associated with any particular pallasitic phase other than its host olivine crystals, as the number of overgrowths in contact with each other phase roughly mirrors their relative abundances at host olivine grain boundaries (Fig. 3a). Additionally, the phase in contact with phosphoran overgrowths does not exert control over their size (Fig. 3b).

Within phosphoran overgrowths, striking oscillatory zoning in P and Si is present on a fine (<10 μm) scale (Fig. 4). Zones of uniform P content range from linear to serrate in shape, with both morphologies often juxtaposed concentrically. Overgrowth regions proximal to the host grain are generally more P-rich and more serrate than distal regions. The serrations are most readily discernible in overgrowths imaged with EDS element mapping, but contrast adjustments to the BSE images suggest that these zoning patterns are present within all overgrowths. The contact between phosphoran and P-free olivine is always sharp, with no interruption to the macroscopic contours of the host grain boundary where overgrowths occur (Figs. 2 and 4). On the other hand, overgrowth margins at the metal contact may be smooth but are more often irregular, truncating the internal zoning (e.g., Fig. 2a, inset). The olivine grains and their phosphoran overgrowths are also cut by an irregularly branching network of ≤3 μm wide metal veins (Fig. 2), a texture attributed to shock in meteorites (Stöffler et al. 1991).

Geochemical analysis

Major and minor elements

Springwater phosphoran olivine ranges from 2.07 to 7.13 wt% P_2O_5 (for full results from 179 EMP analyses, see online depository[1]). The variable P_2O_5 content within single overgrowths and sharp decrease to ~0 wt% at the contact to the host grain can be seen in traverses roughly perpendicular to the grain

[1] Deposit item AM-15-105344, Supplemental Material. Deposit items are free to all readers and found on the MSA web site, via the specific issue's Table of Contents (go to http://www.minsocam.org/MSA/AmMin/TOC/).

boundary (Fig. 5). The inverse relationship between P_2O_5 and SiO_2 content—and a similar correlation of half the magnitude between P_2O_5 and MgO+FeO+MnO—indicates the substitution of P for Si with vacancies in the octahedral site to balance charge (Buseck and Clark 1984; Boesenberg and Hewins 2010). This substitution mechanism is supported in the full data set by the slope of –0.52 with increasing P for Mg+Fe+Mn cations (R^2 = 0.47), –1.01 for Si cations (R^2 = 0.93), and very nearly 0 for P+Si cations (Fig. 6). As P is incorporated into the structure, Fe and Mn appear to be preferentially excluded as compared with Mg. The rate of Fe decrease with increasing P accounts for 34% of the total rate of divalent cation decrease, while Fe occupies only 17% of the octahedral sites on average; similarly, the rate of Mn decrease represents 1% of the total, though Mn occupies only 0.37% of the sites. These discrepancies may be due to the greater size of octahedrally coordinated Fe^{2+} (0.78 Å) and Mn^{2+} (0.83 Å) as compared with Mg^{2+} (0.72 Å) (Henderson 1982).

Trace elements

Full trace element data, including minimum detection limits, can be found in the online depository. We tested the possibility of P accomodation in olivine through coupled substitutions with 3+ cations (Milman-Barris et al. 2008) by plotting V and Cr concentrations against P levels (Fig. 7); Al could not be compared as it

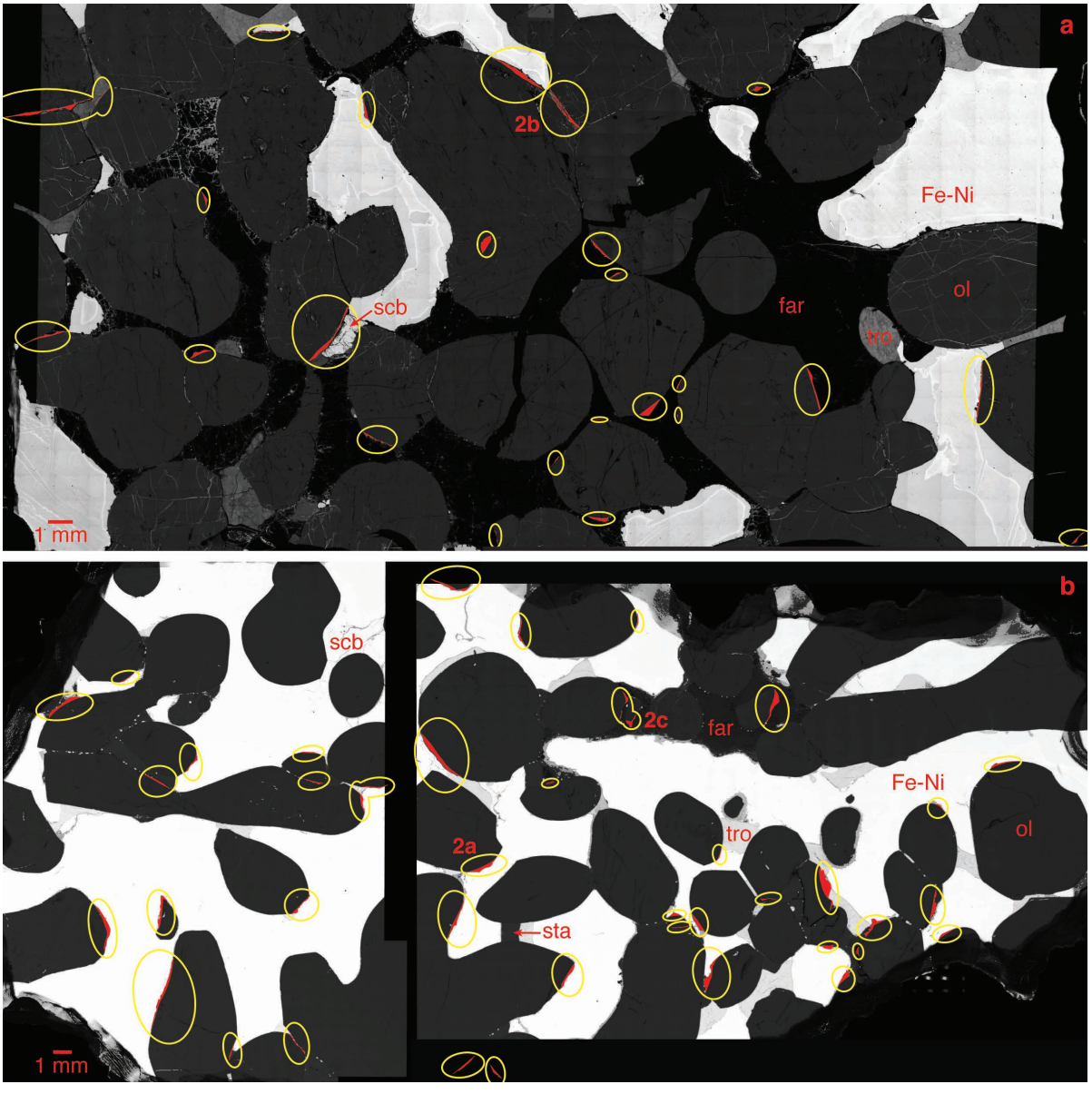

Figure 1. BSE images. Springwater contains abundant phosphoran olivine (shaded in red and indicated by yellow ellipses) as partial overgrowths on the large olivine grains. Overgrowths are randomly distributed, irrespective of spatial variations in accessory mineralogy: compare large clot of farringtonite in matrix (**a**) with predominantly metal matrix (**b**). Phases indicated are olivine (ol), taenite and kamacite (Fe-Ni), farringtonite (far), troilite (tro), stanfieldite (sta), and schreibersite (scb). (Locations marked 2a, 2b, and 2c correspond to Fig. 2.)

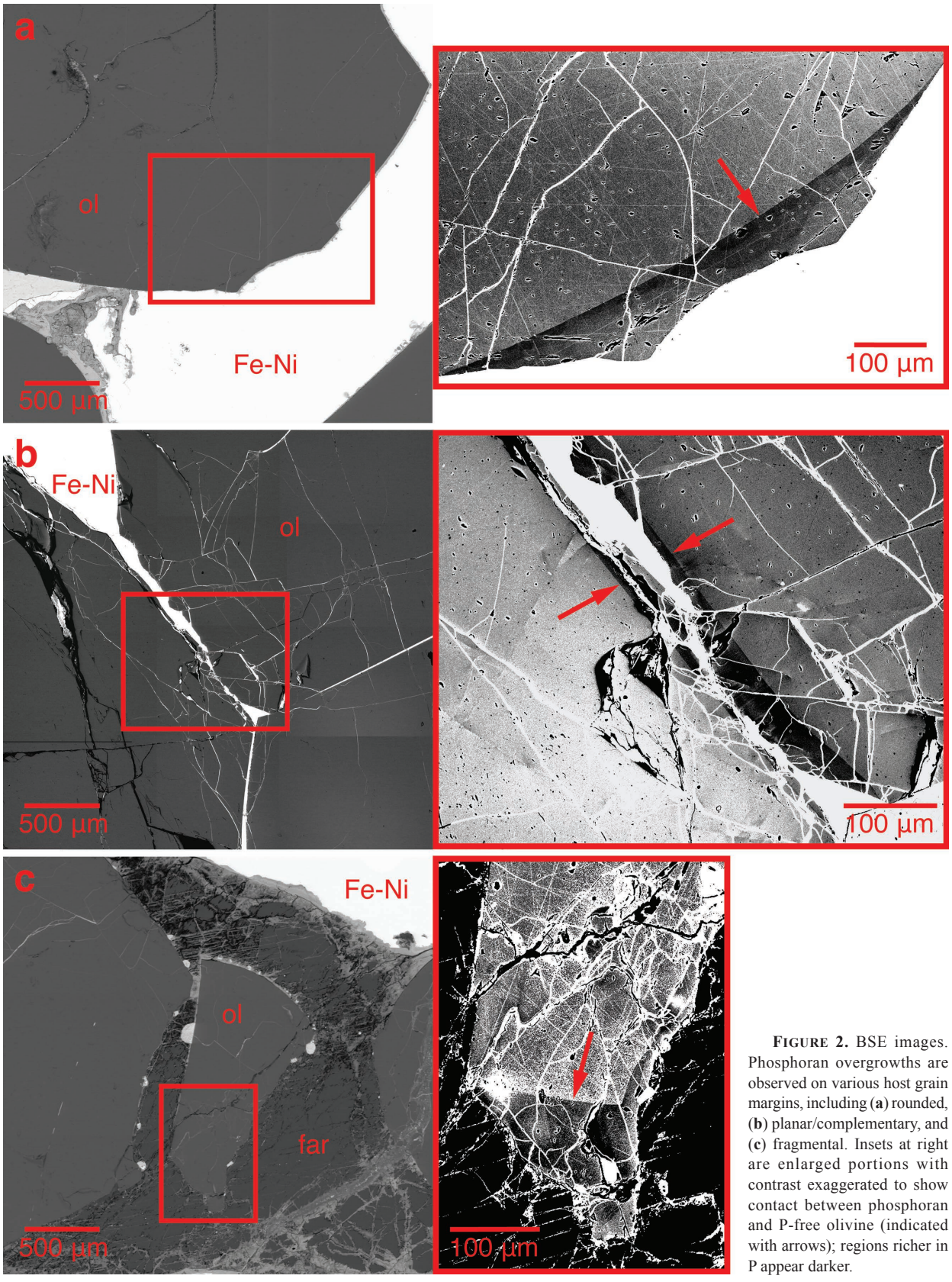

FIGURE 2. BSE images. Phosphoran overgrowths are observed on various host grain margins, including (**a**) rounded, (**b**) planar/complementary, and (**c**) fragmental. Insets at right are enlarged portions with contrast exaggerated to show contact between phosphoran and P-free olivine (indicated with arrows); regions richer in P appear darker.

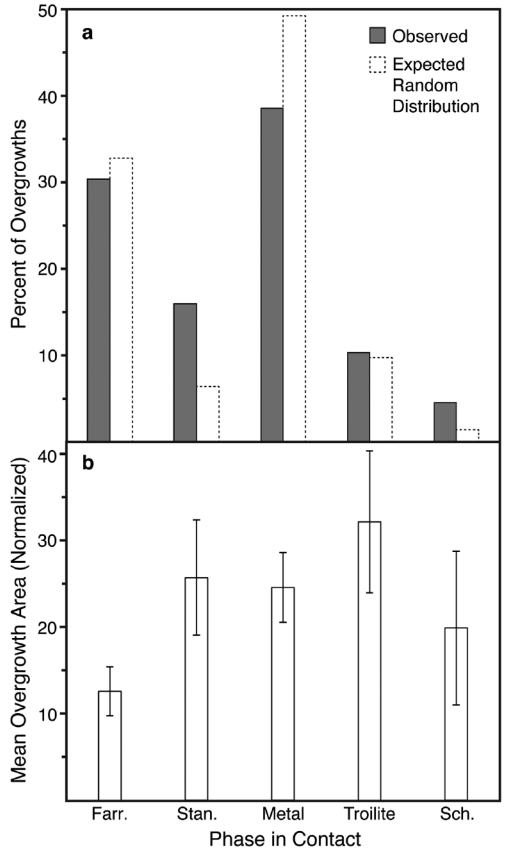

FIGURE 3. (**a**) Percent of overgrowths observed in contact with farringtonite, stanfieldite, metal, troilite, and schreibersite, as compared with the expected profile assuming a random distribution of overgrowths (based on the estimated relative abundances of each phase at host olivine grain margins). (**b**) Mean area (approximated by the maximum width of an overgrowth multiplied by its length along the host grain boundary) of overgrowths observed in contact with each phase, normalized to the area of the largest overgrowth (uncertainties shown are standard errors of the mean).

was not detectable above background. No relationship exists between V and P_2O_5 or Cr and P_2O_5 ($R^2 = 0.01$ in both cases), suggesting this substitution mechanism does not operate in the case of Springwater phosphoran olivine.

DISCUSSION

Boesenberg and Hewins (2010) propose that phosphoran olivine crystallizes via the following pathway at ~1000 °C, an oxygen fugacity of IW-1, and 0.1 MPa (italics indicate metastable intermediates):

$$\begin{aligned} &FeP + (Mg,Fe)_2SiO_{4OLIV} + O_2 >> \\ &\textit{(Mg,Fe,□)}_2\textit{(Si,P)O}_{\textit{4OLIV}} + \textit{SiO}_{\textit{2TRID}} + Si - P_{MELT} >> \\ &(Mg,Fe)_2SiO_{4OLIV} + (Mg,Fe)_3(PO_4)_{2PHOS} + Si - P_{MELT} \end{aligned} \quad (1)$$

Though pallasites almost certainly resided at pressures greater than 0.1 MPa because of their burial depth (Yang et al. 2010), Springwater olivine has been estimated at f_{O_2} ~IW (Righter et al. 1990). Assuming a reaction sequence in Springwater similar to Equation 1, the reduced stability of schreibersite during cooling (Buseck and Holdsworth 1977; Olsen and Fredriksson 1966) could have caused P enrichment in a residual silicate melt surrounding the olivine crystals, the persistence of which has been postulated as a necessary condition for creating the rounded grain boundaries (Ohtani 1983; Boesenberg et al. 2012). Crystallization of the phosphoran olivine from a melt, as opposed to via replacement reactions below the solidus (Buseck 1977), is strongly supported by the concentric P zoning and sharp contacts to the uninterrupted contours of host grains. The metastable character of the phosphoran overgrowths is corroborated by irregular outer margins that cross-cut the P zoning in a manner suggestive of dissolution (e.g., Fig. 2a, inset). Though farringtonite [$Mg_3(PO_4)_2$] is an end product of this reaction sequence as proposed by Boesenberg and Hewins (2010), the vast majority of Springwater farringtonite likely derives from other sources because it is not

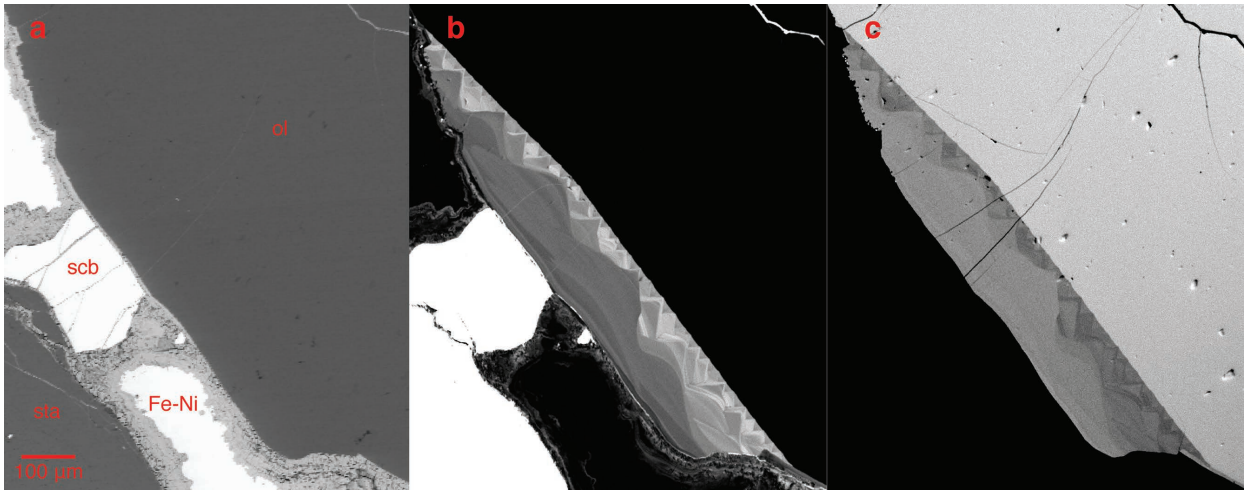

FIGURE 4. (**a**) BSE image of a typical phosphoran overgrowth. Fine-scale oscillatory zoning in linear and serrate patterns is revealed through WDS maps for (**b**) P*K*α and (**c**) Si*K*α.

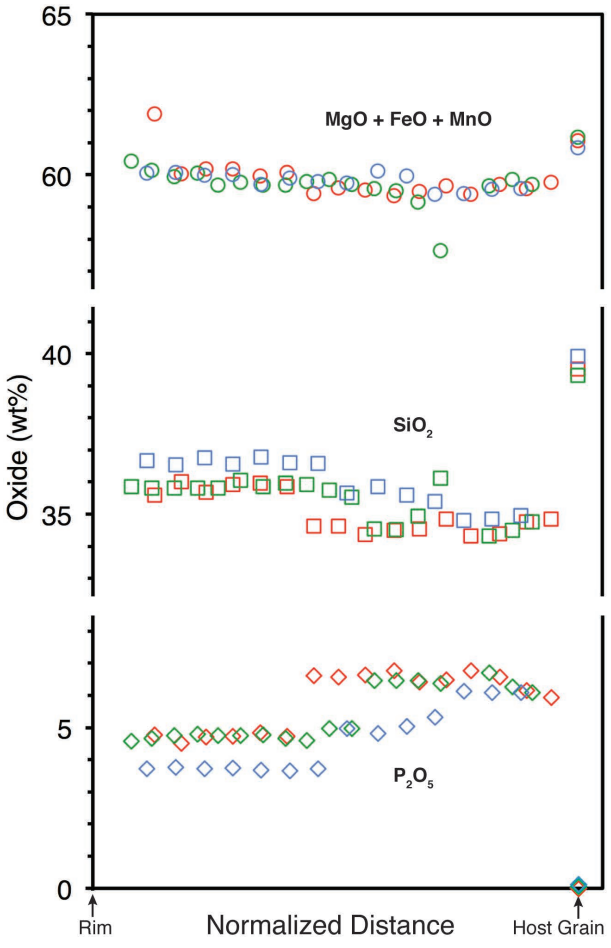

FIGURE 5. EMP analyses across three phosphoran overgrowths (different colors) show correlated variations in P_2O_5, SiO_2, and MgO+FeO+MnO with distance (normalized to total width of overgrowth) and an abrupt transition to the nearly P-free composition of the host olivine crystal (all symbols are larger than 1σ error based on counting statistics).

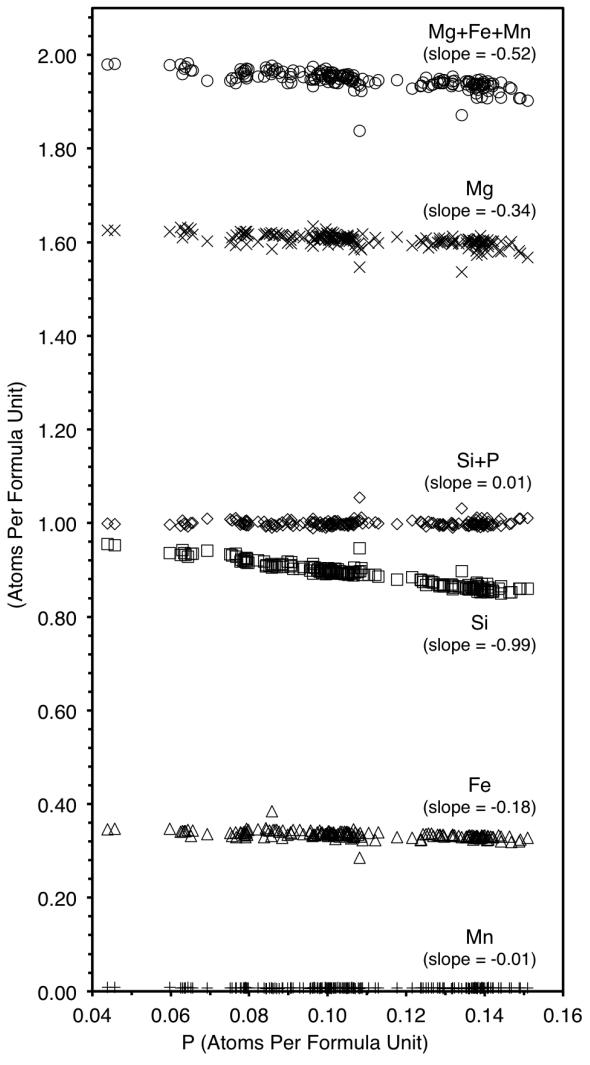

FIGURE 6. Data from 179 EMP analyses in phosphoran olivine show consistent relationships between P, Si, and octahedral site cations (all symbols are larger than 1σ error based on counting statistics).

spatially correlated with phosphoran olivine—and moreover, a mass-balance problem is apparent in the orders of magnitude greater volume of farringtonite (e.g., Fig. 1a) than that of any conceivable original extent of phosphoran overgrowths.

The dramatic compositional zoning we observe within Springwater's phosphoran olivine begs a more sophisticated discussion of its formation mechanisms. Oscillatory zoning in P at trace levels is common in igneous olivine, though the mechanisms that produce these features are not fully understood (Milman-Barris et al. 2008). Although zoning of this nature can develop due to wildly fluctuating P concentrations in the melt, we rule out such a scenario without any plausible mechanism that might account for repeated melt influx to the Springwater pallasitic region. Furthermore, Cr and V systematics of individual overgrowths appear to reflect simple fractional crystallization trends from closed melt reservoirs (Fig. 8). Under such conditions, Cr/V would be expected to rise with increasing Cr because olivine/melt partition coefficients at ~IW are ~0.6 for Cr (Gaetani and Grove 1997) and ~0.5 for V (Mallmann and O'Neill 2009). Despite the structural changes expected when significant P_2O_5 is incorporated into olivine (Boesenberg and Hewins 2010), the presence of highly linear trends in Cr/V vs. Cr in the expected direction suggests that relative partitioning of Cr and V in Springwater phosphoran olivine is broadly similar to that expected for olivine with little or no P. Given this evidence for formation of phosphoran overgrowths from closed melt pockets, we offer two alternative interpretations of the oscillatory zoning that rest on the more plausible premise of changing crystallization rate.

Possibly, periods of rapid crystal growth allow greater incorporation of incompatible P cations but also deplete the adjacent melt layer of the major elements that form olivine, thereby causing intervals of slower crystallization of olivine poorer in P (Milman-Barris et al. 2008). Modeling by Watson and Müller (2009) demonstrates disequilibrium uptake of incompatible elements where crystallization occurs more quickly than cations are able to diffuse away through the boundary layer of melt. If this

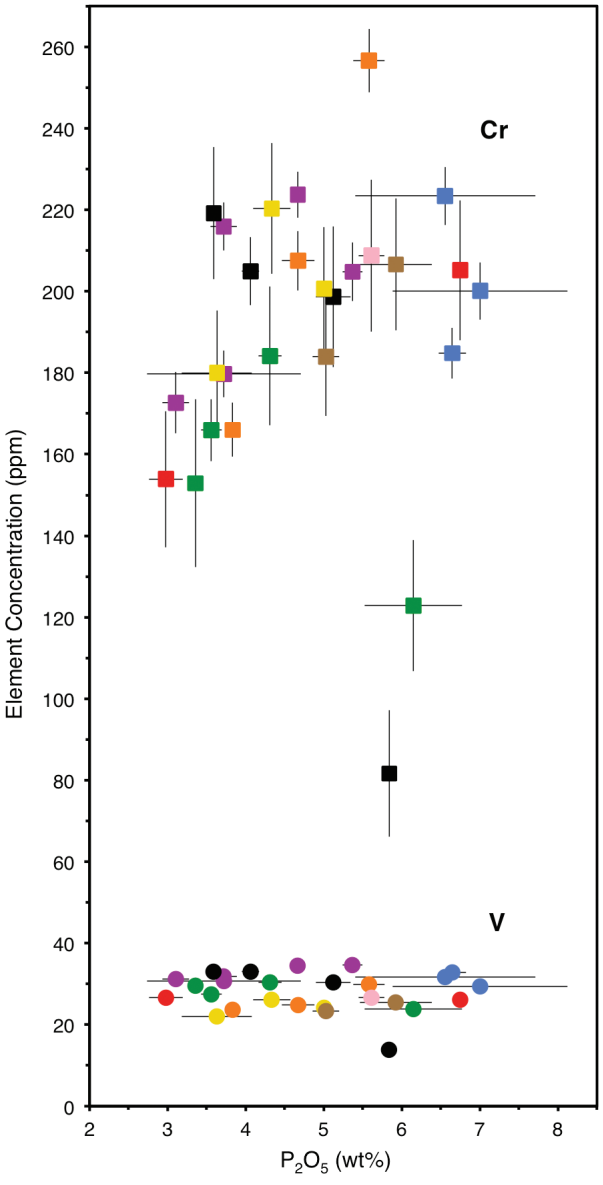

FIGURE 7. Cr and V concentrations (uncertainties are 1σ error based on counting statistics) vs. P_2O_5 (uncertainties are half the difference between the EMP analyses at each end of laser ablation line, plus 1σ error based on counting statistics), with analyses from single overgrowths shown as the same color.

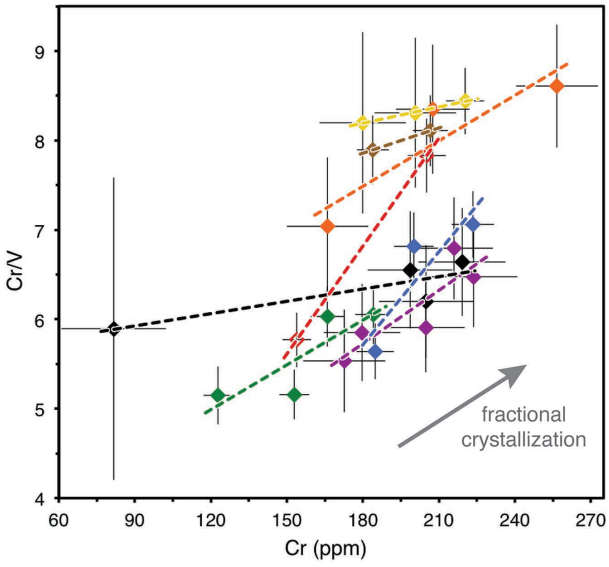

FIGURE 8. Cr/V vs. Cr concentration, with analyses from single overgrowths shown as the same color (1σ error based on counting statistics shown). Arrow indicates rough approximation of the trend expected during fractional crystallization from a closed melt reservoir, given slightly higher compatibility of Cr than V in olivine.

process operated in Springwater, the overgrowth zones highest in P (indicating the most rapid crystallization) might be expected to show enrichment in other incompatible elements also limited by diffusivity in the melt. However, no strongly incompatible trace elements are detectable in Springwater phosphoran olivine, making it difficult to evaluate this hypothesis. It is also challenging to assess the rate of P diffusion in the melt because many of the variables known to control diffusivity, such as temperature, pressure, and melt composition (Hofmann 1980), are not well constrained.

On the other hand, the fine-scale zoning in P may be related not to limitations on diffusion through the melt, but rather to unique properties of P within the actively forming crystal lattice. The structural differences of a newly formed lattice layer as compared to the inner lattice are often associated with higher equilibrium cation concentrations, thus allowing "growth entrapment" of normally incompatible constituents when additions to the lattice are rapid enough (Watson and Liang 1995). During the crystallization of the Springwater phosphoran olivine overgrowths, more frequent lattice additions may have produced zones richer in P while periods of slower growth may have allowed each layer more time to transition toward the lower-P equilibrium concentration of the inner lattice. The absence of correlated Cr or V enrichments with P may simply reflect "normal" equilibrium partitioning behavior for these elements even in the outer lattice.

The unusual serrate morphology of the P zoning is also a likely consequence of growth rate. The most similar pattern reported in the literature is "fir tree zoning" in calcite cements, thought to develop through abrupt changes in the relative growth rate of adjacent crystal sectors (Raven and Dickson 1989); however, it is unlikely the pattern is crystallographically controlled in Springwater. Not only are serrations interspersed laterally on individual crystal faces, rather than forming stacked triangles along sector boundaries as in fir tree zoning, but also serrate, linear, and intermediate forms are often observed within single overgrowths. Because serrate zones tend to predominate close to the host grain interface, and often are the most phosphorus-rich, these patterns may be a record of high-density crystal nucleation and rapid growth due to significant undercooling (Swanson 1977). A net decrease in the rate of crystallization (superimposed on the smaller-scale rate oscillations) may have produced increasingly linear and P-poor layers as the overgrowths advanced outward.

Combined with the evidence for rapid crystallization from a melt, textural relationships can be used to bracket the relative timing of phosphoran olivine formation. Not only do the phosphoran overgrowths overprint the rounding of host grain margins, but they also post-date the opening of linear interstices between adjacent well-annealed olivine crystals, as well as the formation of isolated fragmental grains. The latest possible time of phosphoran olivine formation is constrained by the cross-cutting metal shock veins, which in turn must have been generated before Springwater cooled below 360 °C considering the preserved paleomagnetic signature in pallasitic metal (Tarduno et al. 2012; Bryson et al. 2015). It is probable that phosphoran olivine formed far earlier than this, in fact, since the uninterrupted contours of host olivine grain boundaries indicate overgrowth crystallization from the original residual melt that facilitated macroscopic grain rounding (Ohtani 1983; Boesenberg et al. 2012) rather than from any melt formed subsequent to initial cooling below the solidus. Phosphoran olivine thus likely crystallized prior to the long slow cooling period inferred from the delicate Widmanstätten texture (Owen and Burns 1939) and Ni diffusion profiles (Yang et al. 2010) within the metal phases.

IMPLICATIONS

The macroscopic rounding of the olivine grains is taken as evidence that Springwater experienced at least 10–100 m.y. above ~1250 °C (Scott 1977; Saiki et al. 2003). Below ~700 °C, Main Group pallasites are estimated to have cooled at 2.5–18 °C/m.y (5.1 ± 0.7 °C/m.y for Springwater; Yang et al. 2010). What event could have occurred between these extended periods of near-stasis in the local environment to trigger the episode of extremely rapid crystallization necessary to crystallize and preserve phosphoran olivine? One possible mechanism for interrupting the gradual cooling trajectory is an impact to the parent body. Either substantial surface excavation or the generation of impact melt (thus initiating a convective cooling regime) could dramatically accelerate the cooling of the pallasitic region. Reaccretion of the disrupted material and/or the shift back to a conductive cooling regime after melt solidification may have facilitated the transition to the low cooling rates recorded by the metal phases; the dissolution of outer margins of phosphoran overgrowths implies that cooling rates began to decrease even before temperatures had fallen significantly below the solidus.

An impact to the Main Group pallasite parent body that brought temperatures too low for the efficient rounding of olivine grains is independently indicated by Springwater's pervasive slight partings between grains whose contours imply annealing in contact with olivine rather than metal. While the grains with mutual boundaries are generally aligned according to their [100] axes, the slightly separated grains are more misaligned but still definitively non-random, suggesting that these latter grains broke apart from clusters after cooling had proceeded too far for their complementary-shaped boundaries to become rounded (Fowler-Gerace et al. in preparation). The isolated fragmental grains lend additional support for an impact subsequent to cooling below ~1250 °C. The overprinting phosphoran overgrowths may have crystallized immediately following the event responsible for these olivine textural modifications, although the observations do not exclude their formation after another later impact.

Alternatively, the formation of phosphoran olivine overgrowths could be explained by viscous entrainment of olivine clusters in convection currents within the molten metal of the pallasitic region, perhaps causing multiple cycles of crystallization and dissolution as host olivine grains were repeatedly transported through a temperature range just straddling the solidus. Viscous entrainment is possible when the viscous forces are greater than the buoyancy forces. Simple calculations with reasonable estimates of the relevant parameters for Springwater reveal that the metal must convect at a velocity greater than 1 m/s to entrain olivine. Using convection scaling laws from Carrigan (1987), we estimate that the upper bound for flow velocity in a convecting pallasitic region 300 m to 30 km in size (the highest value chosen as the difference in estimated burial depth between the Esquel and Imilac pallasites; Tarduno et al. 2012) would be 0.28 to 2.3 m/s, respectively. Entrainment of olivine into the convective flow is therefore only possible with a large unified body of molten metal; whether transport of olivine grains across this distance would also yield a temperature differential conducive to cycles of crystallization and only partial dissolution of the metastable phosphoran overgrowths is unknown.

However, such a scenario may not explain the presence of phophoran overgrowths on the fragmental olivine of the Brahin pallasite (Buseck 1977). It is difficult to imagine that olivine grains entrained within molten metal convecting faster than 1 m/s would not become rounded through mutual collisions over millions of years [the assumed duration in the absence of impact-related modification of the slow cooling trajectory reported by Yang et al. (2010)]. Additionally, the suggested convection mechanism may be incongruous with the serrate shapes of only the earliest growth zones of Springwater's phosphoran olivine. One would expect the degree of undercooling to be roughly the same each time olivine clusters were carried to shallower depths, therefore promoting high-density nucleation for all generations of phosphoran olivine. A suddenly accelerated cooling rate due to impact, on the other hand, may be more consistent with the zoning features suggestive of one crystal nucleation event during extremely rapid initial growth, followed by generally slowing crystallization and smaller rate oscillations due to boundary layer effects (Watson and Müller 2009) or growth entrapment (Watson and Liang 1995).

Multiple impacts to the Main Group pallasite parent body subsequent to its differentiation but prior to solidification of the pallasitic metal is not implausible. Using the present-day impact probability per year on Earth modeled by Le Feuvre and Wieczorek (2011), the probability of impact P by bodies with radius r over time t to the Main Group pallasite parent body can be estimated to an order of magnitude by

$$P(r,t) \simeq 10^{-8}\left(\frac{r}{5\text{km}}\right)^{-13/5}\left(\frac{R}{R_E}\right)^2\left[\frac{(2GR^2\rho/V^2)+1}{(2GR_E^2\rho_E/V_E^2)+1}\right]\left(\frac{a_{\text{Pallasite}}}{1\text{AU}}\right)^2\left(\frac{f(t)}{10^{10}\text{g/yr}}\right) \quad (2)$$

where R is the radius of the target body, G is the universal gravitational constant, ρ is the bulk density of the body, V is the orbital velocity, a is the heliocentric distance, $f(t)$ is the terrestrial impact mass flux as a function of time (Koeberl

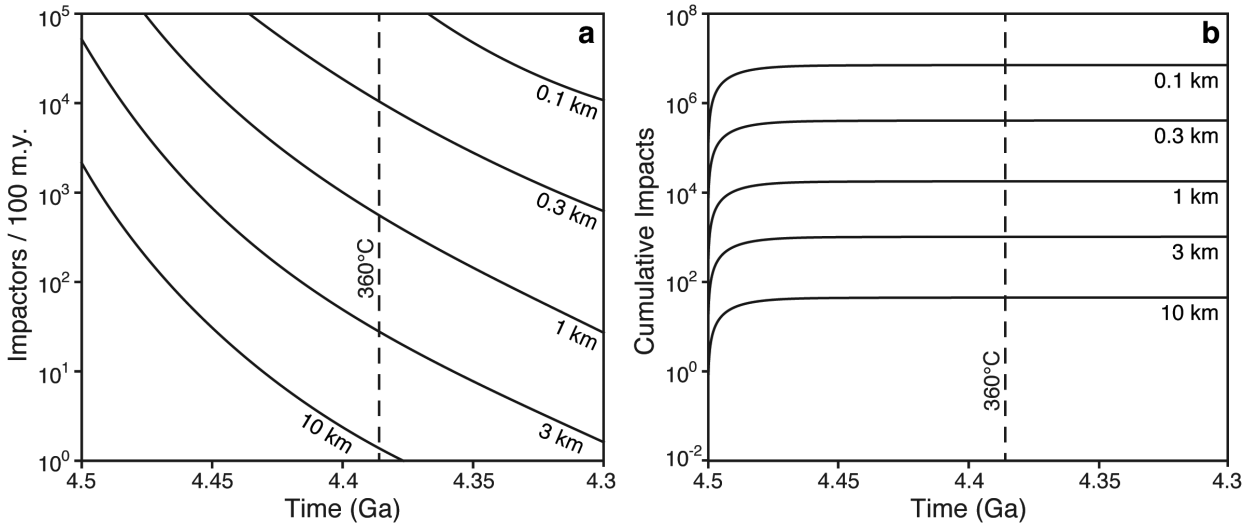

Figure 9. Number of impactors per 100 m.y. (**a**) and cumulative number of impacts (**b**) expected to occur on a 200 km radius planetesimal in the asteroid belt as a function of time, with different possible impactor radii indicated. Core-mantle differentiation of planetesimals is thought to have occurred within 10 m.y. of Solar System formation (Wadhwa et al. 2006), so 4.5 Ga can be taken as a conservative estimate of the latest time the upper mantle region of the Main Group pallasite parent body differentiated to nearly monomineralic olivine cumulates. The latest possible time that impacts could account for the textures we observe in Springwater is shown with a dashed line indicating the approximate time that Springwater cooled below 360 °C (~180 m.y. after accretion, assuming 40 km burial depth; Tarduno and Cottrell 2013) and began to preserve a paleomagnetic signature within the tetrataenite cloudy zone (Bryson et al. 2015).

2006), and the subscript *E* denotes values for Earth. Figure 9 shows the impactor flux, assuming 200 km radius for the Main Group pallasite parent body (Tarduno et al. 2012), heliocentric distance approximated by the asteroid belt, and average density 3.5 g/mL. Before Springwater cooled through 360 °C (after which reheating is impossible owing to the preservation of a coherent paleomagnetic signature; Bryson et al. 2015), tens of 10 km radius impactors and orders of magnitude more smaller impactors are predicted to have encountered the parent body.

The textural relationships among phosphoran olivine, host olivine grains, and metal in Springwater imply up to two late impacts to the Main Group pallasite parent body, besides the impact proposed to have initially integrated metal into the olivine-rich upper mantle region (Tarduno et al. 2012). One additional impact may have induced the breakup of olivine clusters and accelerated cooling rates substantially, preventing the efficient rounding of olivine margins exposed to metal as well as promoting the rapid crystallization and preservation of phosphoran overgrowths. A second impact associated with temperatures below the olivine solidus [~1320 °C at the eutectic with farringtonite (Boesenberg and Hewins 2010)] but above that of the metal matrix [~950 °C based on ~12.7% each Ni and S as in Springwater (Buseck 1977; Starykh and Sineva 2012)] could have fractured olivine grains and their overgrowths, creating space that would naturally fill with molten metal. The absence of phosphoran olivine in the majority of Main Group pallasites may be related to lower local P concentrations or simply a lack of detection by previous investigators.

Acknowledgments

The authors acknowledge the Louise Hawley Stone acquisition grant and Canadian Cultural Property Export and Review board funding for the purchase of the Springwater pallasite sample, Ian Nicklin (Royal Ontario Museum) for facilitating sample preparation, Brian Joy (Queen's University) and Yanan Liu (University of Toronto) for assistance with electron microprobe analyses, Colin Bray (University of Toronto) for aid in LA-ICP-MS data acquisition, James Brenan for advice regarding trace element data collection and interpretation of results, and Bob Tian for aid in modeling impactor flux to the Main Group pallasite parent body. Funding for the research was from a NSERC Discovery Grant (to K.T.T.), a peer review grant from the Louise Hawley Stone Trust, the Canadian Space Agency Astromaterials Training and Research Opportunities (ASTRO) Graduate Student Incentive Award, and the University of Toronto Connaught Scholarship.

References cited

Agrell, S.O., Charnley, N.R., and Chinner, G.A. (1998) Phosphoran olivine from Pine Canyon, Piute Co., Utah. Mineralogical Magazine, 62, 265–269.

Anderson, A.T., and Greenland, L.P. (1969) Phosphorus fractionation diagram as a quantitative indicator of crystallization differentiation of basaltic liquids. Geochimica et Cosmochimica Acta, 33, 493–505.

Armstrong, J.T. (1988) Quantitative analysis of silicate and oxide minerals: comparison of Monte Carlo, ZAF and phi-rho-z procedures. Microbeam Analysis, 23, 239–246.

Boesenberg, J.S. (2006) Wrought iron from the *USS Monitor*: Mineralogy, petrology, and metallography. Archaeometry, 48, 613–631.

Boesenberg, J.S., and Hewins, R.H. (2010) An experimental investigation into the metastable formation of phosphoran olivine and pyroxene. Geochimica et Cosmochimica Acta, 74, 1923–1941.

Boesenberg, J.S., Delaney, J.S., and Hewins, R.H. (2012) A petrological and chemical reexamination of Main Group pallasite formation. Geochimica et Cosmochimica Acta, 89, 134–158.

Brunet, F., and Chazot, G. (2001) Partitioning of phosphorus between olivine, clinopyroxene and silicate glass in a spinel lherzolite xenolith from Yemen. Chemical Geology, 176, 51–72.

Bryson, J.F.J., Nichols, C.I.O., Herrero-Albillos, J., Kronast, F., Kasama, T., Alimadadi, H., van der Laan, G., Nimmo, F., and Harrison, R.J. (2015) Long-lived magnetism from solidification-driven convection on the pallasite parent body. Nature, 517, 472–475.

Buseck, P.R. (1977) Pallasite meteorites—Mineralogy, petrology and geochemistry. Geochimica et Cosmochimica Acta, 41, 711–740.

Buseck, P.R., and Clark, J. (1984) Zaisho—A pallasite containing pyroxene and phosphoran olivine. Mineralogical Magazine, 48, 229–235.

Buseck, P.R., and Holdsworth, E. (1977) Phosphate minerals in pallasite meteorites. Mineralogical Magazine, 41, 91–102.

Carrigan, C.R. (1987) The magmatic Rayleigh number and time dependent convection in cooling lava lakes. Geophysical Research Letters, 14, 915–918.

Floss, C. (2002) Queen Alexandra Range 93148: A new type of pyroxene pallasite?

Meteoritics & Planetary Science, 37, 1129–1139.
Gaetani, G.A., and Grove, T.L. (1997) Partitioning of moderately siderophile elements among olivine, silicate melt, and sulfide melt: Constraints on core formation in the Earth and Mars. Geochimica et Cosmochimica Acta, 61, 1829–1846.
Goodrich, C.A. (1984) Phosphoran pyroxene and olivine in silicate inclusions in natural iron-carbon alloy, Disko Island, Greenland. Geochimica et Cosmochimica Acta, 48, 2769–2771.
——— (2003) Petrogenesis of olivine-phyric shergottites Sayh al Uhaymir 005 and Elephant Moraine A79001 lithology A. Geochimica et Cosmochimica Acta, 67, 3735–3772.
Heinrich, K.F.J. (1966) X-ray absorption uncertainty. In T.D. McKinley, K.F.J. Heinrich, and D.B. Wittry, Eds., The Electron Microprobe, p. 296–377. Wiley, New York.
——— (1986) Mass absorption coefficients for electron probe microanalysis. In J.B. Brown and R.H. Packwood, Eds., Proceedings of the 11th International Congress on X-ray Optics and Microanalysis, p. 67–119. London, Canada.
Henderson, P., Ed. (1982) Structural controls of element distribution, p. 102–155. In Inorganic Geochemistry, Pergamon, Oxford.
Henke, B.L., and Ebisu, E.S. (1974) Low energy X-ray and electron absorption within solids (100–1500 eV region). In C.L. Grant, C.S. Barrett, J.B. Newkirk, and C.O. Ruud, Eds., Advances in X-Ray Analysis, 17, p. 150–213. Plenum, New York.
Hofmann, A.W. (1980) Diffusion in natural silicate melts: A critical review. In R.B. Hargraves, Ed., Physics of Magmatic Processes, p. 385–418. Princeton University Press, New Jersey.
Hsu, W. (2003) Minor element zoning and trace element geochemistry of pallasites. Meteoritics & Planetary Science, 38, 1217–1241.
Koeberl, C. (2006) The record of impact processes on the early Earth: A review of the first 2.5 billion years. In W.U. Reimold and R.L. Gibson, Eds., Processes on the Early Earth, 405, p. 1–22. Geological Society of America Special Paper, Boulder, Colorado.
Le Feuvre, M., and Wieczorek, M.A. (2011) Nonuniform cratering of the Moon and a revised crater chronology of the inner Solar System. Icarus, 214, 1–20.
Leitch, C.A., Steele, I.M., Hutcheon, I.D., and Smith, J.V. (1979) Minor elements in pallasites: Zoning in Springwater olivine. Lunar and Planetary Science Conference, 10, 716–718.
Mallmann, G., and O'Neill, H.St.C. (2009) The crystal/melt partitioning of V during mantle melting as a function of oxygen fugacity compared with some other elements (Al, P, Ca, Sc, Ti, Cr, Fe, Ga, Y, Zr and Nb). Journal of Petrology, 50, 1765–1794.
Mallmann, G., O'Neill, H.St.C., and Klemme, S. (2009) Heterogeneous distribution of phosphorus in olivine from otherwise well-equilibrated spinel peridotite xenoliths and its implications for the mantle geochemistry of lithium. Contributions to Mineralogy and Petrology, 158, 485–504.
McKibbin, S.J., O'Neill, H.S.C., Mallmann, G., and Halfpenny, A. (2013) LA-ICP-MS mapping of olivine from the Brahin and Brenham meteorites: Complex elemental distributions in the pallasite olivine precursor. Geochimica et Cosmochimica Acta, 119, 1–17.
Milman-Barris, M.S., Beckett, J.R., Baker, M.B., Hofmann, A.E., Morgan, Z., Crowley, M.R., Vielzeuf, D., and Stolper, E. (2008) Zoning of phosphorus in igneous olivine. Contributions to Mineralogy and Petrology, 155, 739–765.
Ohtani, E. (1983) Formation of olivine textures in pallasites and thermal history of pallasites in their parent body. Physics of the Earth and Planetary Interiors, 32, 182–192.
Olsen, E., and Fredriksson, K. (1966) Phosphates in iron and pallasite meteorites. Geochimica et Cosmochimica Acta, 30, 459–470.
Owen, E.A., and Burns, B.D. (1939) X-ray study of some meteoric irons. The Philosophical Magazine, 28, 497–512.
Pouchou, J.L., and Pichoir, F. (1985) PAP (phi-rho-Z) procedure for improved quantitative microanalysis. In J.T. Armstrong, Ed., Microbeam Analysis, p. 104–106. San Francisco Press, California.
Raven, M.J., and Dickson, J. (1989) Fir-tree zoning—An indicator of pulsed crystallization in calcite cement crystals. Sedimentary Geology, 65, 249–259.
Righter, K., Arculus, R.J., Delano, J.W., and Paslick, C. (1990) Electrochemical measurements and thermodynamic calculations of redox equilibria in pallasite meteorites: Implications for the eucrite parent body. Geochimica et Cosmochimica Acta, 54, 1803–1815.
Saiki, K., Laporte, D., Vielzeuf, D., Nakashima, S., and Boivin, P. (2003) Morphological analysis of olivine grains annealed in an iron-nickel matrix: Experimental constraints on the origin of pallasites and on the thermal history of their parent bodies. Meteoritics & Planetary Science, 38, 427–444.
Scott, E.R.D. (1977) Formation of olivine-metal textures in pallasite meteorites. Geochimica et Cosmochimica Acta, 41, 693–710.
Sonzogni, Y., Devouard, B., Provost, A., and Devidal, J.-L. (2009) Olivine-hosted melt inclusions in the Brahin pallasite. In Meteoritics and Planetary Science Supplement, p. 5070, 72nd Annual Meeting of the Meteoritical Society, Nancy, France.
Starykh, R.V., and Sineva, S.I. (2012) Study of the liquidus and solidus surfaces of the quaternary Fe–Ni–Cu–S system: V. Refinement and addition of the data on the ternary Fe–Ni–S and Fe–Ni–Cu phase diagrams. Russian Metallurgy, 3, 189–194.
Stöffler, D., Keil, K., and Scott, E.R.D. (1991) Shock metamorphism of ordinary chondrites. Geochimica et Cosmochimica Acta, 55, 3845–3867.
Swanson, S.E. (1977) Relation of nucleation and crystal-growth rate to the development of granitic textures. American Mineralogist, 62, 966–978.
Tarduno, J.A., and Cottrell, R.D. (2013) Paleomagnetism of the Springwater pallasite: Further evidence for a dynamo in the Main Group pallasite parent body. 44th Lunar and Planetary Science Conference, Texas.
Tarduno, J.A., Cottrell, R.D., Nimmo, F., Hopkins, J., Voronov, J., Erickson, A., Blackman, E., Scott, E.R.D., and McKinley, R. (2012) Evidence for a dynamo in the main group pallasite parent body. Science, 338, 939–942.
Tropper, P., Recheis, A., and Konzett, J. (2004) Pyrometamorphic formation of phosphorus-rich olivines in partially molten metapelitic gneisses from a prehistoric sacrificial burning site (Ötz Valley, Tyrol, Austria). European Journal of Mineralogy, 16, 631–640.
Wadhwa, M., Srinivanson, G., and Carlson, R.W. (2006) Timescales of planetesimal differentiation in the early solar system. Meteoritics and the Early Solar System II, 715–731.
Wang, Y., Hua, X., and Hsu, W. (2007) Petrogenesis of opaque assemblages in the Ningqiang carbonaceous chondrite. Science in China Series D: Earth Sciences, 50, 886–896.
Wasson, J.T., and Choi, B.G. (2003) Main-group pallasites: Chemical composition, relationship to IIIAB irons, and origin. Geochimica et Cosmochimica Acta, 67, 3079–3096.
Wasson, J.T., Lange, D.E., and Francis, C.A. (1999) Massive chromite in the Brenham pallasite and the fractionation of Cr during the crystallization of asteroidal cores. Geochimica et Cosmochimica Acta, 63, 1219–1232.
Watson, E.B., and Liang, Y. (1995) A simple model for sector zoning in slowly grown crystals: implications for growth rate and lattice diffusion, with emphasis on accessory minerals in crustal rocks. American Mineralogist, 80, 1179–1187.
Watson, E.B., and Müller, T. (2009) Non-equilibrium isotopic and elemental fractionation during diffusion-controlled crystal growth under static and dynamic conditions. Chemical Geology, 267, 111–124.
Yang, J., Goldstein, J.I., and Scott, E.R.D. (2010) Main-group pallasites: Thermal history, relationship to IIIAB irons, and origin. Geochimica et Cosmochimica Acta, 74, 4471–4492.

Manuscript received March 4, 2015
Manuscript accepted June 15, 2015
Manuscript handled by Bruce Watson